APPENDIX
SUPPLEMENTARY FIGURES & TABLES

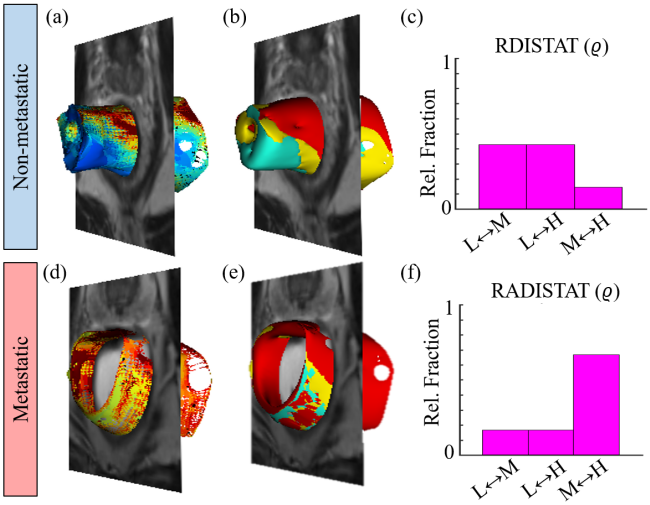

Fig. S1. Representative 3D visualizations of radiomic and RADISTAT expression maps for RCa patients with metastatic disease (top row) and non-metastatic disease (bottom) after chemoradiation; from the discovery cohort. Visually apparent differences across the (a),(d) radiomic volume-rendered heatmaps for GLCM difference variance are captured via sub-regions of (b),(e) high, medium, and low radiomic expression via RADISTAT. Histograms reveal distinctive spatial phenotypes within the rectal wall that accurately discriminate between (c) metastatic and (f) non-metastatic rectal cancers after chemoradiation.

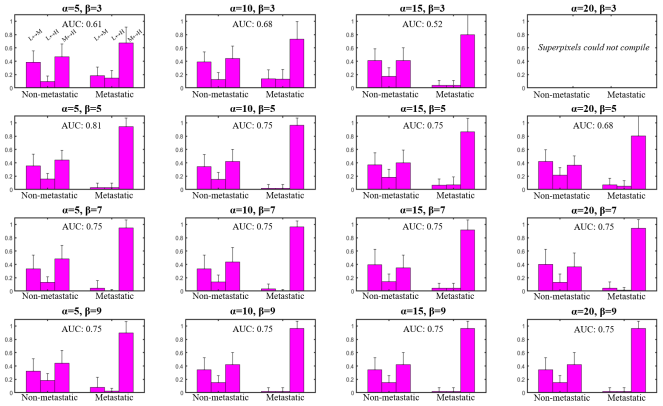

Fig. S2. Median histograms for 2D RADISTAT (based on GLCM inertia) per outcome group and for each α-β combination in RCa patients, indicating consistent trends between metastatic and non-metastatic disease.

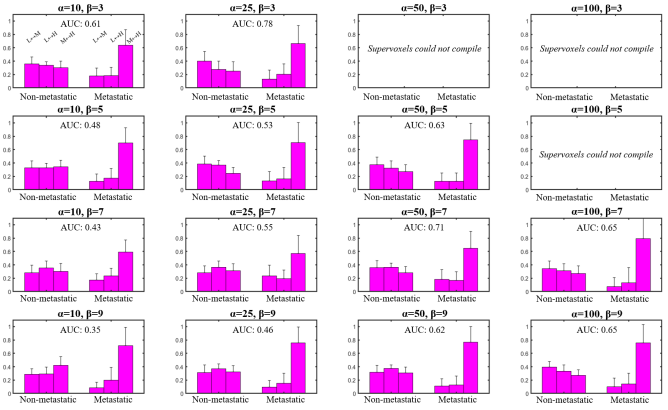

Fig. S3. Median histograms for 3D RADISTAT (based on GLCM difference variance) per outcome group and for each α-β combination in RCa patients, with consistent trends between metastatic and non-metastatic disease.

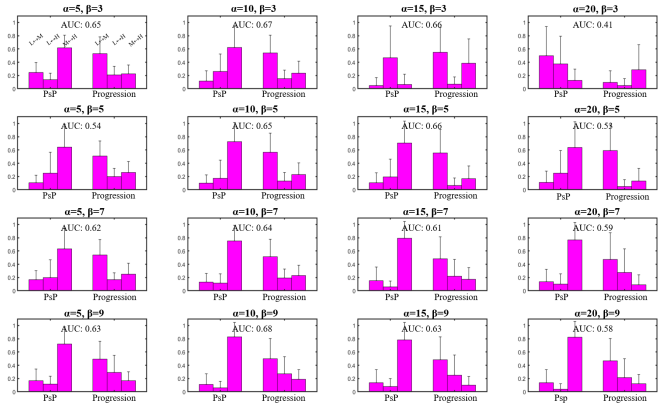

Fig. S4. Median histograms for 2D RADISTAT (based on GLCM energy) per outcome group and for each α-β combination in GBM patients, with consistent trends between PsP and tumor progression.

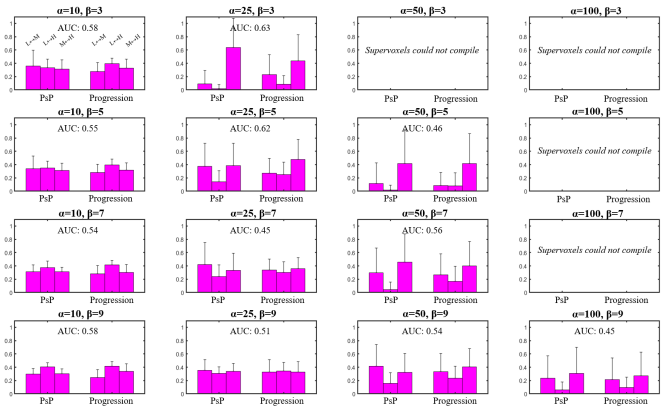

Fig. S5. Median histograms for 3D RADISTAT (based on GLCM correlation) per outcome group and for each α-β combination in GBM patients, with consistent trends between PsP and tumor progression.

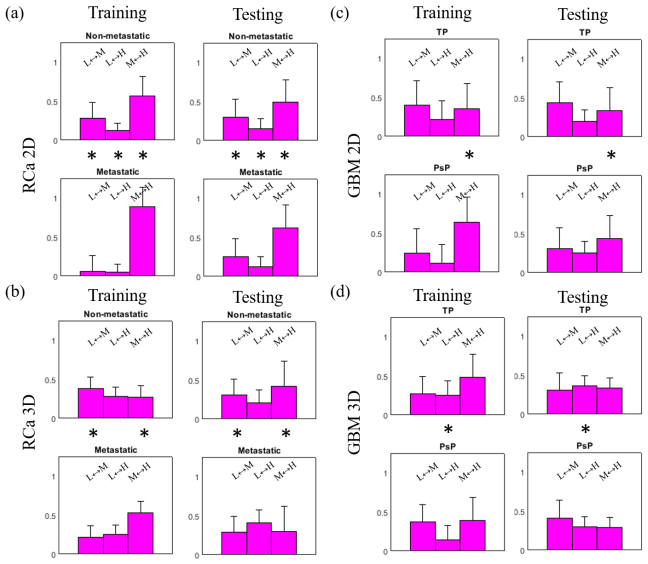

Fig. S6. Testing for statistically significant differences between RADISTAT components. Asterisks (*) indicate statistical significance using non-parametric ranksum test ($p \leq 0.05$, corrected for multiple comparisons) between corresponding vertical pairs of spatial adjacency components between different outcomes. (a)-(b) RCa classification task. (c)-(d) GBM classification task.